Phase diagram and thermodynamic properties of solid magnesium in the quasiharmonic approximation

J. D. Althoff,* P. B. Allen, and R. M. Wentzcovitch†
Department of Physics, State University of New York at Stony Brook, Stony Brook, New York 11794

John A. Moriarty
Lawrence Livermore National Laboratory, University of California, Livermore, California 94550
(Received 4 August 1992; revised manuscript received 16 February 1993)

Using a family of volume-dependent interatomic pair potentials derived from first principles, we calculate phonon properties and thermodynamic functions in the quasiharmonic approximation for the hcp and bcc phases of Mg over a wide range of volume and temperature. At atmospheric pressure, the calculated hcp phonon-dispersion curves and thermodynamic properties agree well with experiment. The pressure dependence of the Raman-active transverse-optical phonon mode also agrees well with very recent measurements. At high pressure, the temperature dependence of the hcp-bcc phase line is predicted, with values of the transition pressure ranging from 52 GPa at zero temperature to about 28 GPa at 1000 K.

I. INTRODUCTION

Magnesium is unique among the alkaline-earth metals in that it melts at atmospheric pressure out of the hcp structure; Be, Ca, and Sr all exhibit temperature-induced phase transitions from a close-packed structure (hcp for Be, fcc for Ca and Sr) to bcc prior to melting, while Ba is already bcc at zero temperature.[1,2] All of the alkali metals also melt out of the bcc structure, as do all of the early transition metals.[1,2] In Mg the bcc phase is found only at high pressure, with a room-temperature hcp→bcc transition observed at about 50 GPa.[3] This phase transition was actually predicted theoretically[4,5] and the zero-temperature aspects of the transition have been well studied by a variety of first-principles methods.[4–6] In addition, there has been a semiempirical calculation of the pressure-temperature phase diagram below 100 GPa which suggests a vary rapid temperature dependence to the hcp-bcc phase line.[7] The purpose of this paper is to similarly extend the first-principles analysis to finite temperature. Specifically, we present here a study of the thermodynamic properties of hcp and bcc magnesium in the quasiharmonic phonon approximation and a corresponding calculation of the hcp-bcc phase line to 1000 K.

The zero-temperature energetics of Mg have been successfully addressed by both nonperturbative and perturbative total-energy methods based on the local-density-approximation (LDA) to density-functional theory.[8] The nonperturbative linear-muffin-tin-orbital[4,5] (LMTO) and *ab initio* pseudopotential[6] (AP) methods and the perturbative generalized pseudopotential theory[4,5] (GPT) yield results for the hcp-bcc transition pressure and volume in good agreement with each other and with experiment, as shown in Table I. The LMTO and AP methods employ full electronic-structure calculations which exploit the high symmetry of the zero-temperature environment. To extend such calculations to the phase diagram at finite temperature would require thousands of Cray hours of computer time. The GPT method, on the other hand, employs expansions of the electron density and total energy which are not constrained by symmetry and is ideally suited to address the finite-temperature problem. In the present work, we utilize a real-space expansion of the GPT total energy developed to second order in a nonlocal electron-ion pseudopotential. In this formulation the total energy can be expressed as a pure volume term plus a pairwise sum over a two-ion central-force interatomic potential:

$$E_{\rm tot}(\mathbf{R}_1 \cdots \mathbf{R}_N) = NE_{\rm vol}(\Omega) + \frac{1}{2}\sum_{i,j}{}' v_2(R_{ij},\Omega) , \quad (1)$$

TABLE I. Calculated $T=0$ properties of Mg compared with experiment: $E_{\rm coh}$, cohesive energy; a, hcp lattice constant; c/a ratio; B_0, bulk modulus; P_T and Ω_T/Ω_0, hcp→bcc transition pressure and relative atomic volume. Theoretical values do not include the zero-point vibrational contribution; experimental values are room-temperature data.

Property	Band theory		GPT		Experiment
	LMTO[a]	AP[b]	Previous[c]	Present[d]	
$\lvert E_{\rm coh}\rvert$ (eV)		1.62		1.60	1.51[e]
a (bohr)		6.01		6.12	6.07[f]
c/a		1.623		1.621	1.624[f]
B_0 (GPa)		37		32.6	35.4[e]
P_T (GPa)	57	60	50	54	50±6[g]
Ω_T/Ω_0	0.56	0.57	0.58	0.58	0.59±0.02[g]

[a]Linear-muffin-tin-orbital calculations from Ref. 5.
[b]*Ab initio* pseudopotential calculations from Ref. 6.
[c]Reciprocal-space calculations in the empty-d-band limit from Ref. 5; LMTO pressure scale was used to obtain P_T.
[d]Real-space calculations in the simple-metal limit via Eq. (1).
[e]Reference 14.
[f]Reference 13.
[g]Reference 3.

where $\Omega \equiv V/N$ is the atomic volume, $R_{ij} \equiv |\mathbf{R}_i - \mathbf{R}_j|$ is the distance between ions i and j, and the prime on the summation excludes the $i=j$ term. The functions $E_{\rm vol}(\Omega)$ and $v_2(r,\Omega)$ both depend on the atomic volume Ω but are independent of structure. Consequently, at constant volume all dependence of the total energy on ion position $\mathbf{R}_i$ is explicit in Eq. (1) and it is straightforward to calculate quasiharmonic phonons directly from the pair potential v_2 for any crystal structure. The principal additional approximation contained in Eq. (1), and not in the LDA electronic-structure methods, is the neglect of three-ion and higher potentials which are third order and higher in the electron-ion pseudopotential. In Mg this approximation is well justified by the free-electron nature of the metal and the corresponding weakness of the pseudopotential. This is confirmed in the experimental hcp phonon spectrum which can be accurately fit by an axially symmetric force-constant model.[9]

Both the zero-temperature total energy and the phonons can be calculated as a function of volume via Eq. (1) and thus all thermodynamic functions may be readily evaluated in the quasiharmonic approximation as a function of volume and temperature. Anharmonic effects are expected to be small in Mg and are here neglected. We have verified that this is a good approximation through appropriate anharmonic cell-model calculations. The equilibrium phase diagram in the solid (for conditions of constant temperature and pressure) is calculated by finding the structure of lowest Gibbs free energy. The equation of state, bulk modulus, specific heat, thermal expansion coefficient, and Grüneisen parameter are calculated from appropriate thermodynamic derivatives.

In Sec. II, we first discuss the calculation of the required functionals $E_{\rm vol}$ and v_2 entering Eq. (1). Then, in Sec. III, we consider the application of these quantities to obtain phonons and the hcp-bcc phase line for Mg. Additional thermodynamic properties are considered in Sec. IV and we conclude in Sec. V.

II. FIRST-PRINCIPLES INTERATOMIC POTENTIALS

The hcp→bcc phase transition in Mg is part of a general sequence of high-pressure structural phase transitions in the third-period metals (Na, Mg, Al, and Si) that are driven by the gradual lowering and occupation of $3d$ states from above the Fermi level.[4,5] This effect is particularly subtle in these metals because the d states in question are initially free electron in character and only slowly develop a transition-metal-like localized character under ultrahigh compression. In the context of the GPT method, the zero-temperature energetics of Mg have previously been treated in both the simple-metal limit[4] (plane-wave basis) and the empty-d-band limit[5] (mixed basis of plane waves and localized d states). The latter permits an explicit treatment of any transition-metal-like sp-d hybridization present. In Mg below about 100 GPa (1 Mbar), however, this effect is essentially negligible and so we may work here entirely in the simple-metal limit.

The simple-metal limit of the GPT is a refined first-principles version of conventional pseudopotential perturbation theory. This limit, as well as all others of the GPT, has been fully developed within the framework of LDA quantum mechanics[10] and requires only the atomic number Z_a (=12 for Mg) and valence Z (=2 for Mg) as input. The total energy may be cast in either a reciprocal-space representation, as done previously for Mg,[4,5] or in an equivalent real-space representation, as in Eq. (1). We have opted here for a real-space description to permit a parallel study of the actual mechanism of the hcp-bcc transition via molecular dynamics.[11] In the simple-metal limit, the pair potential v_2 is in the form of a screened Coulomb potential given by

$$v_2(r,\Omega)=\frac{(Z^*e)^2}{r}\left[1-\frac{2}{\pi}\int_0^\infty F_N(q,\Omega)\frac{\sin(qr)}{q}dq\right], \tag{2}$$

where Z^* is an effective valence and F_N is the normalized energy–wave-number characteristic

$$F_N(q,\Omega)=\frac{q^2\Omega^2}{4\pi(Z^*e)^2}\left[-\frac{4}{(2\pi)^3}\int_{k<k_F}\frac{|\langle \mathbf{k}+\mathbf{q}|w|\mathbf{k}\rangle|^2}{\epsilon_{\mathbf{k}}-\epsilon_{\mathbf{k}+\mathbf{q}}}d\mathbf{k}+\frac{4\pi e^2}{q^2}\{[1-G(q)][n_{\rm scr}(q)]^2+G(q)[n_{\rm oh}(q)]^2\}\right] \tag{3}$$

with

$$\langle \mathbf{k}+\mathbf{q}|w|\mathbf{k}\rangle=\frac{4\pi e^2}{q^2}\{-Z/\Omega+[1-G(q)][n_{\rm scr}(q)+n_{\rm oh}(q)]\}+\langle \mathbf{k}+\mathbf{q}|w_{\rm core}|\mathbf{k}\rangle\ . \tag{4}$$

Here w is an optimized and self-consistently screened nonlocal pseudopotential with an inner-core component $w_{\rm core}$; $n_{\rm scr}$ is the corresponding screening electron density obtained to first order in w; $n_{\rm oh}$ is a localized orthogonalization-hole density arising from the exclusion of the valence electrons from the inner-core region of each ion such that $Z^*=Z-\int n_{\rm oh}(\mathbf{r})d\mathbf{r}$; and $G(q)$ is an exchange-correlation function which here is taken from Ichimaru and Utsumi.[12] The function $F_N(q,\Omega)$ incorporates the effects of electron screening on the pair potential v_2 and is normalized such that $F_N(0,\Omega)=1$. At small separation r, the direct Coulomb interaction will dominate in Eq. (2) and one can expect a steeply repulsive potential $v_2(r)$ [$\equiv v_2(r,\Omega)$ at fixed Ω]. At large r, the direct Coulomb interaction cancels with the electron screening field leaving Friedel oscillations [i.e., $v_2(r)\propto \sin(2k_Fr)/r^3$] arising from the sharp Fermi cutoff at k_F in Eq. (3). In practice, these oscillations can cause

numerical problems in the convergence of real-space sums, and a compromise must be established between an acceptable level of convergence and a tractable calculational scheme. Here we cut off the potential $v_2(r)$ at $8.25R_{\rm WS}$ for each volume $\Omega=4\pi R_{\rm WS}^3/3$; real-space sums then include enough neighbors (536 in the bcc structure and 538 in the hcp structure) that Eq. (1) produces structural energies and phonon frequencies which are both smooth functions of volume and agree with their (highly converged) reciprocal-space counterparts to within a few percent.

The corresponding volume term in Eq. (1) is given by an expression of the form

$$E_{\rm vol}(\Omega)=E_{\rm eg}-\tfrac{1}{2}\Omega B_{\rm eg}+\frac{2\Omega}{(2\pi)^3}\int_{k<k_F}(\langle\mathbf{k}|w_{\rm core}|\mathbf{k}\rangle-\bar{w}_{\rm core})d\mathbf{k}-\frac{(Z^*e)^2}{\pi}\int_0^\infty F_N(q,\Omega)dq+O(w^2)-E_{\rm bind}^{\rm atom}\ . \tag{5}$$

Here $E_{\rm eg}=\frac{3}{5}Z\epsilon_F+Z\epsilon_{\rm xc}$, the kinetic and exchange-correlation energy of the electron gas of density Z/Ω; $B_{\rm eg}$ is the corresponding bulk modulus; $\bar{w}_{\rm core}$ is a Fermi-sea average of $w_{\rm core}$; and the remaining second-order terms involve $F_N(q,\Omega)$ and orthogonalization-hole contributions. The quantity $E_{\rm bind}^{\rm atom}$ is the valence binding energy of the free atom, which may be calculated within the same LDA framework.[10] With the constant $E_{\rm bind}^{\rm atom}$ included, the total energy in Eq. (1) is with respect to separated atoms, i.e., $E_{\rm coh}\equiv E_{\rm tot}/N$ is the cohesive energy of the solid. As shown in Fig. 1, the volume term $E_{\rm vol}$ is the major component of the cohesive energy of Mg near equilibrium, but the rapid increase in $E_{\rm coh}$ at high pressure actually arises from the repulsive part of the pair potential. The volume and pair-potential components of Eq. (1) combine to give an excellent cohesive energy vs volume curve with an equilibrium volume only slightly larger than experiment. As Table I demonstrates, the calculated $T=0$ cohesive properties of hcp Mg at equilibrium based on Eq. (1) agree well both with experiment[13,14] and with LDA electronic structure calculations.[6] In this regard, we have minimized the hcp energy with respect to the c/a axial ratio, finding an equilibrium value of 1.621. As the pressure is raised, we find that this value is changed by less than 1% over the volume range of interest in this paper. We have, therefore, maintained a constant value of 1.62 throughout all the remaining calculations discussed below.

The $T=0$ structural properties of Mg are similarly well calculated by the pair potentials $v_2(r,\Omega)$. The observed hcp structure near equilibrium and the observed bcc structure at high pressure are each correctly predicted to be the lowest-energy phase among all competing metallic structures. Figure 2 displays our calculated hcp-fcc and bcc-fcc cohesive energy differences as a function of volume. These results indicate an hcp→bcc phase transition near $\Omega/\Omega_0=0.6$, where Ω_0 is the observed equilibrium atomic volume. The details of the transition may be calculated by equating hcp and bcc enthalpies ($E_{\rm tot}+PV$, here without zero-point vibrational contributions). The values of the transition pressure and volume so obtained are given in Table I and are seen to agree well both with previous theoretical results[4–6] and with experiment.[3] As expected, we find a very small fractional volume change for this transition, $(\Omega_{\rm bcc}-\Omega_{\rm hcp})/\Omega_{\rm hcp}\simeq-0.005$ or about -0.5%.

Qualitatively, the origin of the hcp→bcc transition can be traced to the behavior of the pair potentials in the vicinity of the near-neighbor shells. Figure 3 shows the pair potentials for Mg calculated at volumes both near zero pressure and near the hcp-bcc transition. Near

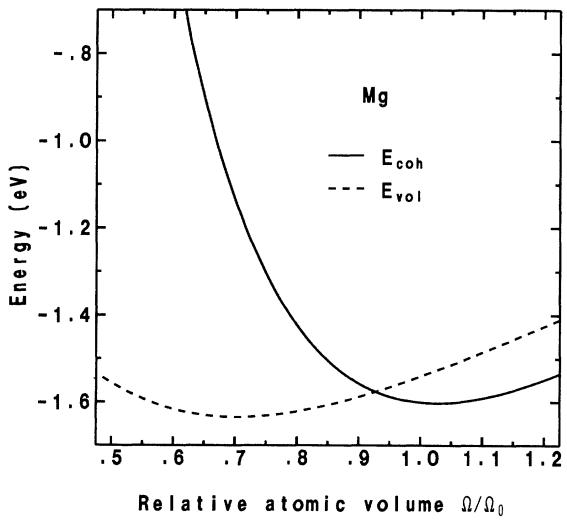

FIG. 1. Volume term $E_{\rm vol}$ and cohesive energy $E_{\rm coh}=E_{\rm tot}/N$ for hcp Mg ($c/a=1.62$) as a function of relative atomic volume, Ω/Ω_0. Here Ω_0 is the observed equilibrium atomic volume (156.8 a.u.).

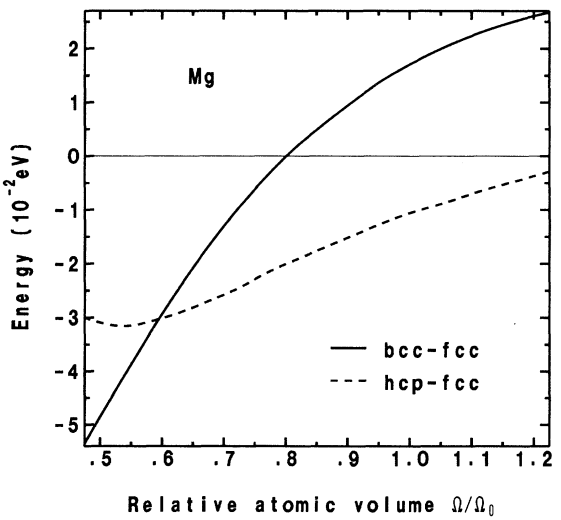

FIG. 2. Zero-temperature hcp-fcc and bcc-fcc cohesive energy differences as a function of relative atomic volume, Ω/Ω_0, with the hcp c/a ratio and Ω_0 as in Fig. 1.

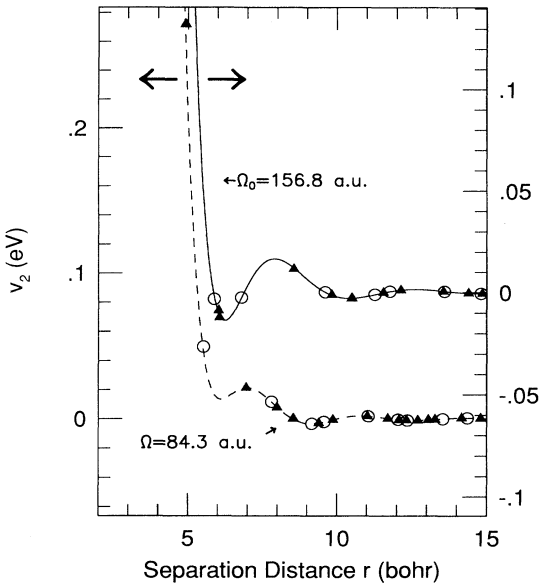

FIG. 3. The pair potential v_2 in Mg for two different volumes: the solid line is at the observed equilibrium volume for the hcp structure ($\Omega_0 = 156.8$ a.u.) and is referenced to the vertical axis on the right-hand side; the dashed line is at a volume 84.3 a.u. (where bcc is stable) and is referenced to the vertical axis on the left-hand side. The triangles (circles) on each curve are near-neighbor distances in the hcp (bcc) structure at the same volume.

$P=0$, the 12 nearest neighbors of the hcp structure lie very close to the first minimum of the potential, while the 8 nearest neighbors and 6 next-nearest neighbors of the bcc structure straddle the minimum on either side, so the bcc energy is clearly higher. (In the hcp structure, the nearest-neighbor distances are $1.805R_{\rm WS}$ and $1.814R_{\rm WS}$ for $c/a=1.62$; in the bcc structure, the nearest-neighbor distance is $1.759R_{\rm WS}$ and the next-nearest-neighbor distance is $2.031R_{\rm WS}$.) As the volume is decreased, the first-neighbor shells of both structures begin to move up the steep repulsive portion of the pair potential and the high number of nearest neighbors for the hcp structure becomes increasingly less favorable. Eventually, Mg can lower its energy by transforming to the less close-packed bcc structure, allowing some of these neighbors to move off the steep portion of the potential and back toward the first minimum, as shown in Fig. 3.

III. PHONONS AND THE hcp-bcc PHASE LINE

In the presence of lattice vibrations at constant volume, the total potential energy of the crystal within the quasiharmonic approximation can be written

$$U=E^0_{\rm tot}+\frac{1}{4}\sum_{i,j}\sum_{\mu,\nu}(u^i_\mu-u^j_\mu)\phi^{ij}_{\mu\nu}(u^i_\nu-u^j_\nu)\ . \tag{6}$$

Here $E^0_{\rm tot}$ is the total energy (1) evaluated for the ideal lattice at equilibrium, u^i_μ is the μth Cartesian component of the displacement from equilibrium of the ith atom, and the force-constant matrix is given by

$$\phi^{ij}_{\mu\nu}=\frac{\partial^2 v_2(R_{ij})}{\partial x_\mu \partial x_\nu}=\delta_{\mu\nu}A(R_{ij})+\frac{x_\mu x_\nu}{R^2_{ij}}B(R_{ij})\ , \tag{7}$$

where x_μ is the μth Cartesian component of $\mathbf{R}_i-\mathbf{R}_j$ and where

$$A(r)\equiv\frac{1}{r}\frac{\partial v_2(r)}{\partial r} \tag{8}$$

and

$$B(r)\equiv\frac{\partial^2 v_2(r)}{\partial r^2}-A(r)\ . \tag{9}$$

All real-space force constants for the crystal can thus be expressed in terms of the first and second derivatives of v_2 evaluated at near-neighbor distances. These derivatives, in turn, can be taken analytically using Eq. (2) and evaluated without difficulty as a function of the separation distance r. It is then straightforward to construct the dynamical matrix, obtain phonon frequencies, and, if desired, calculate the phonon density of states for any given crystal structure. The volume dependence of the phonon frequencies comes both from the volume dependence of the pair potential v_2 and from the volume dependence of the separations R_{ij}.

We have calculated both hcp and bcc phonons for Mg in this manner over the volume range $0.4\Omega_0 \le \Omega \le 1.2\Omega_0$. Figure 4 shows the phonon dispersion curves calculated along the principal symmetry directions in the hcp structure at atmospheric pressure. Good agreement with the experimental results of Pynn and Squires[9] is obtained. The upper panel of Fig. 5 displays the corresponding density of states computed from these dispersion curves. The lower panel shows the density of states for both the hcp and bcc structures at a volume $0.54\Omega_0$ near the hcp→bcc phase transition. A downward shift of the bcc vibrational spectrum with respect to the hcp spectrum is evident in this latter result. In this regard, the bcc phonon spectrum displays the familiar soft $T_1[110]$ modes which are characteristic of the other bcc alkali and alkaline-earth

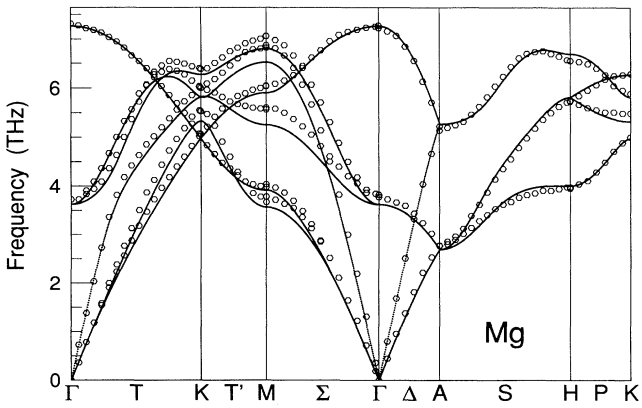

FIG. 4. Phonon dispersion curves along the principal symmetry directions of the hcp structure of Mg at atmospheric pressure. The lines are the results of the present calculations ($c/a=1.62$); the symbols are the experimental data of Ref. 9.

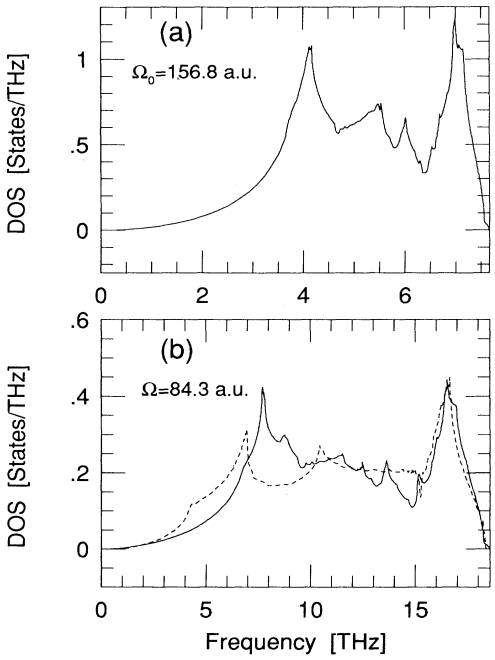

FIG. 5. (a) Calculated phonon density of states for the hcp structure of Mg at atmospheric pressure. (b) Phonon density of states for the hcp (solid line) and bcc (dashed line) structures at $\Omega/\Omega_0=0.54$, where the bcc structure is stable (at $T=0$).

metals and corresponds to a small C' shear elastic constant. It is interesting to note that C' decreases in magnitude as the volume is increased and passes through zero at about $\Omega/\Omega_0=0.93$ or a pressure of about 4 GPa at $T=0$. Thus, the bcc structure is predicted to be unstable at larger volumes and lower pressures, consistent with the absence of even a metastable bcc phase at atmospheric pressure.

Very recently, it has also become possible to obtain quantitative experimental information on phonons at high pressure in metals with two or more atoms per unit cell (e.g., hcp) via Raman spectroscopy in the diamond-anvil cell.[15] After our calculations were completed, we were pleased to learn that Olijnyk had made the first measurements of the transverse-optic (TO) Raman frequency in hcp Mg to 50 GPa.[16] In Fig. 6, we compare our predicted ($\mathbf{q}=0$) TO frequency as a function of pressure with his data. The agreement is clearly very good and provides direct evidence that our calculated phonons indeed remain accurate at high pressure.

From a knowledge of the quasiharmonic phonon frequencies $\nu_\lambda(\mathbf{q})$ as a function of volume for a given structure, one can then compute thermodynamic quantities as a function of volume and temperature. In particular, the Helmholtz free energy is

$$F(V,T)=E^0_{\rm tot}+k_BT\sum_{\mathbf{q},\lambda}\ln\{2\sinh[h\nu_\lambda(\mathbf{q})/(2k_BT)]\}\ , \tag{10}$$

where both $E^0_{\rm tot}$ and $\nu_\lambda(\mathbf{q})$ are implicit functions of volume and where the sum is over all phonon wave vectors $\mathbf{q}$ and branches λ in the first Brillouin zone of the lattice. The pressure P is calculated as the negative volume derivative of F at fixed T, $P=-(\partial F/\partial V)_T$, and the entropy S as the negative temperature derivative of F at fixed V, $S=-(\partial F/\partial T)_V$. Under conditions of constant temperature and pressure, the thermodynamically stable phase is that with the lowest Gibbs free energy, $G=F+PV$. Figure 7 shows the solid portion of the magnesium phase diagram to 1000 K which we have calculated by equating Gibbs energies of the hcp and bcc phases. At $T=0$ we obtain a transition pressure P_T of 52 GPa,

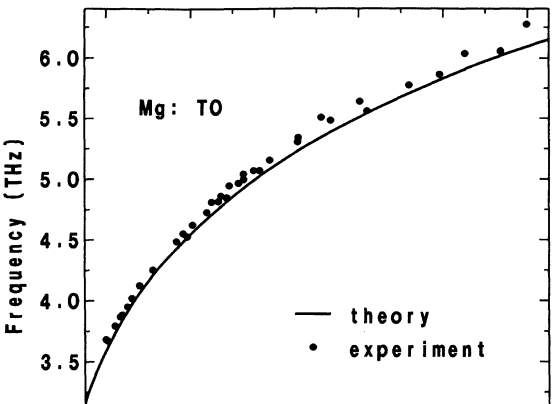

FIG. 6. Transverse-optic (TO) Raman frequency in hcp Mg as a function of pressure. The solid line is the present calculation ($c/a=1.62$) and the points are the experimental data of Ref. 16.

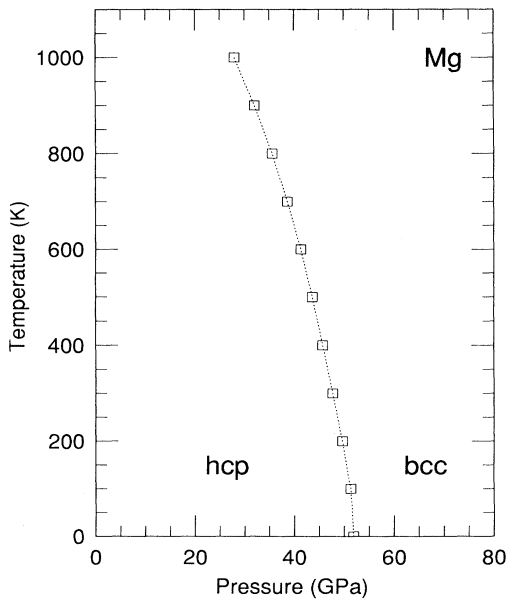

FIG. 7. Solid portion of the Mg phase diagram showing the present theoretical result for the hcp-bcc phase boundary.

which is about 2 GPa less than we found in the absence of zero-point vibrational contributions (Table I). At 300 K the theoretically determined transition pressure is 48 GPa, in good agreement with the experimental value of 50±6 GPa.[3] The negative slope of the hcp-bcc phase line makes possible a temperature-induced phase transition to bcc at constant pressure, with the transition temperature decreasing as the pressure is increased. It has been traditionally argued[17] that the lower phonon frequencies in the bcc structure produce an entropy excess which drives a phase transition to bcc at higher temperatures. This traditional argument appears to be correct in Mg at elevated pressures.

Gibbs' phase rule for a one-component system states that two phases can coexist along a curve in the P-T plane, where the Clausius-Clapeyron equation,

$$\frac{dP_T}{dT}=\frac{\Delta S}{\Delta V}=\frac{S_{\rm bcc}-S_{\rm hcp}}{V_{\rm bcc}-V_{\rm hcp}}\ , \tag{11}$$

specifies the slope of the coexistence curve. For a pressure-induced hcp→bcc phase transition, $\Delta V<0$. Therefore, the negative slope of the calculated phase boundary implies that $\Delta S>0$, i.e., that the entropy of the bcc phase is higher than that of the hcp phase, in accord with the aforementioned soft bcc phonon arguments and as has been verified by direct calculation of the hcp and bcc entropies. At $T=0$ the entropies of both phases must vanish by the third law of thermodynamics since both phases are perfectly ordered. This is ensured by Eq. (10) and the phase line is thus perpendicular to the pressure axis at their intersection. (Note that classically the entropy difference at $T=0$ can be nonzero and the phase boundary need not approach the pressure axis at a right angle: quantum effects force this requirement.)

To verify the adequacy of our quasiharmonic calculation of the hcp-bcc phase line, we have computed anharmonic free-energy corrections to Eq. (10) for both phases using a standard cell model[18] and repeated the entire calculation. We indeed find the net impact of anharmonic effects on the phase line to be very small at all temperatures, with the transition pressure lowered by only about 0.1 GPa at 1000 K.

IV. THERMODYNAMIC PROPERTIES

The remaining measurable thermodynamic quantities can be expressed in terms of appropriate volume and temperature derivatives. In calculating such quantities and comparing the results to experiment, it is important to recall that we have treated the metal as if the electrons are always in their ground state (i.e., at $T=0$), so that the electronic contribution to any quantity expressible as a temperature derivative is identically zero in the present theoretical framework. Thus, in comparing such quantities as the specific heat and thermal expansion coefficient with experiment, we must first subtract the electronic component from the experimental results.

Experimentally, the isothermal bulk modulus $B_T=V(\partial^2F/\partial V^2)_T$ for Mg is observed to be only weakly temperature dependent,[19] and this is generally confirmed in our calculations. Our computed $T=0$ value of B_T for the hcp crystal at atmospheric pressure is 31.7 GPa, which is about 1 GPa lower than we obtained in the absence of zero-point vibrational contributions (Table I). The room-temperature experimental value is 35.4 GPa.[14]

Figure 8 compares our calculated thermal expansion coefficient $\beta=B_T^{-1}(\partial P/\partial T)_V$ as a function of temperature for hcp Mg at atmospheric pressure with the experimental data of Refs. 20 and 21. For theories in which the electronic Grüneisen parameter is independent of temperature, the electronic component of β is linear in T at low temperatures and we have used the value of the linear coefficient quoted in Ref. 20 ($3.3\pm0.2\times10^{-9}$ K^{-2}). For comparison, the lattice component is of order 10^{-5} K^{-1}, so that on the scale of Fig. 8, subtracting the electronic component from the experimental data produces a barely perceptible change. The calculated thermal expansion coefficient agrees well with experiment at low temperature but begins to deviate above the Debye temperature (300 K) and at high temperature (900 K) overestimates experiment by almost a factor of 2. We have investigated this discrepancy and found its origin to be basically twofold. First, neglected anharmonic effects do lower the calculated β above the Debye temperature by a significant amount. However, based on our cell-model calculations only about a third of the discrepancy at high temperature can be accounted for in this manner. A second larger effect is the extreme sensitivity of β to our calculated equation of state. As can be seen from Table I, we overestimate the zero-pressure volume of Mg in the present work by a small amount (2.7%), so that in Fig. 8 we are calculating β at volumes which are slightly larger than experiment. In this regard, our equation of state is approximately corrected by subtracting from it a small constant pressure (1.8 GPa) at all volumes. We find that the corrected equation-of-state plus cell-model anharmonic contributions combine to yield an accurate calculated value of β all the way up to about 800 K, as is also shown in Fig. 8.

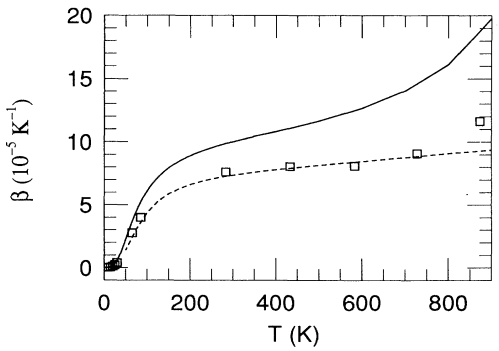

FIG. 8. Thermal expansion coefficient β of hcp Mg at atmospheric pressure. The solid line is the present quasiharmonic calculation ($c/a=1.62$); the symbols are experimental data from Ref. 19 ($T<300$ K) and Ref. 20 ($T>300$ K). The dashed line includes anharmonic and equation-of-state corrections to the quasiharmonic result, as discussed in the text.

We calculate the specific heat at constant volume, c_V, directly from the quasiharmonic phonon spectrum. The specific heat at constant pressure, c_P, is obtained by adding the dilatation term $T\Omega B_T\beta^2$ to c_V. For reference, the dilatation term is only about 2% of c_V at 300 K, but rises monotonically to about 25% of c_V at 800 K. The electronic component of the specific heat is here approximated as linear for all temperatures and is subtracted from the experimental data, using a coefficient $\gamma_e = 1.579 \times 10^{-4} k_B$ K^{-1} per atom from Ref. 22. Figure 9 displays our calculated c_P as a function of temperature for hcp Mg at atmospheric pressure. The agreement with experiment[22,23] is generally good, with a small overestimate in the theoretical result at high temperature due mostly to our overestimate of β, as discussed above. At low temperatures, the effective Debye temperature $\Theta(T)$ defined by

$$c_V = 9k_B \left[\frac{T}{\Theta(T)}\right]^3 \int_0^{\Theta(T)/T} \frac{x^4 e^x}{(e^x-1)^2} dx \tag{12}$$

is perhaps a more illuminating quantity to plot. The inset of Fig. 9 shows $\Theta(T)$ along with the experimental data of Ref. 22.

The isothermal bulk modulus, thermal expansion coefficient, and specific heat at constant volume are connected by the Grüneisen relation

$$\gamma = \frac{V\beta B_T}{Nc_V} = \frac{\Omega\beta B_T}{c_V} , \tag{13}$$

which defines the Grüneisen parameter γ. As expected, our calculated values of γ are only weakly temperature dependent, with the high-temperature limit rapidly approached above the Debye temperature. At atmospheric pressure we obtain $\gamma = 1.7$ for hcp Mg as compared with the experimental value of 1.6. The calculated volume dependence of γ is displayed in Fig. 10.

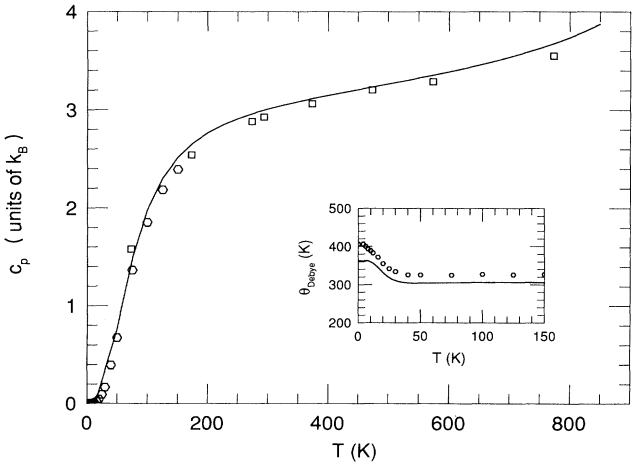

FIG. 9. Specific heat at constant pressure c_p for hcp Mg at atmospheric pressure. The solid line is the present calculation ($c/a = 1.62$); the hexagons and squares are experimental data from Refs. 21 and 22, respectively. Inset: low-T behavior of the effective Debye temperature (see text) with the notation the same.

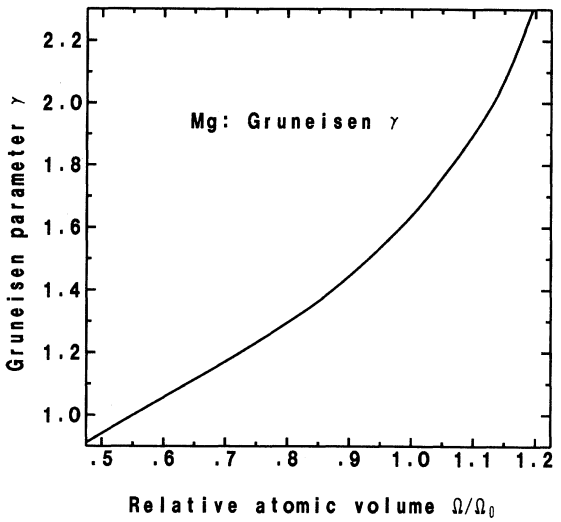

FIG. 10. Calculated high-temperature Grüneisen parameter γ for hcp Mg ($c/a = 1.62$) as a function of relative atomic volume, Ω/Ω_0. As in Figs. 1 and 2, Ω_0 is the observed equilibrium atomic volume.

V. CONCLUSIONS

The structural, vibrational, and thermodynamic properties of Mg are all well described by the present first-principles interatomic potentials derived from the simple-metal limit of generalized pseudopotential theory. The calculated $T = 0$ properties, including the transition pressure and volume of the hcp→bcc phase transition, agree with both experiment and full LDA electronic structure calculations. We have studied here the temperature dependence of the hcp-bcc phase line and the thermodynamic properties of hcp Mg to 1000 K in the quasiharmonic approximation. The hcp→bcc transition pressure is predicted to rapidly decrease with increasing temperature, in qualitative agreement with the earlier semiempirical calculation of Pelissier.[7] In closely related work, the same interatomic potentials have been used to simulate the hcp→bcc transition in Mg using molecular-dynamics techniques.[11] With regard to the vibrational and thermodynamic properties of hcp Mg, we have obtained good quantitative agreement with experiment for all quantities except the thermal expansion coefficient β above the Debye temperature. Deviations with experiment for β at high temperatures appear to be due to a combination of neglected anharmonic effects and extreme sensitivity to small errors in the equation of state.

The high-temperature ($T > 1000$ K) portion of the Mg phase diagram, including the melting curve, is under current investigation. A preliminary calculation suggests that the hcp-bcc phase line should end in a triple point on the melting curve in the vicinity of 6 GPa and 1250 K. If this is indeed the case, it may be possible in the future to experimentally access the entire temperature-induced se-

quence hcp→bcc→liquid in measurements at modest pressure.

ACKNOWLEDGMENTS

Work at Lawrence Livermore National Laboratory was performed under the auspices of the U.S. Department of Energy under Contract No. W-7405-Eng-48. Work at Stony Brook was supported by the Division of Materials Sciences, U.S. Department of Energy, under Contract No. DE-AC02-76CH00016. We thank Rici Yu for providing us with a copy of his code to compute dynamical matrices from force constants. We also thank Dr. Helmut Olijnyk for sharing his Raman data with us prior to publication and for permission to quote the results in Fig. 6.

---

*Present address: Sandia National Laboratories, Livermore, California 94550.

†Present address: The Cavendish Laboratory, Madingly Road, Cambridge CB3 0HE, England.

[1]L.-G. Liu and W. A. Bassett, *Elements, Oxides, and Silicates: High Pressure Phases with Implications for the Earth's Interior* (Oxford University Press, New York, 1986).

[2]D. A. Young, *Phase Diagrams of the Elements* (University of California Press, Berkeley, 1991).

[3]H. Olijnyk and W. B. Holzapfel, Phys. Rev. B **31**, 4682 (1986).

[4]J. A. Moriarty and A. K. McMahan, Phys. Rev. Lett. **48**, 809 (1982).

[5]A. K. McMahan and J. A. Moriarty, Phys. Rev. B **27**, 3235 (1983).

[6]R. M. Wentzcovitch and M. L. Cohen, Phys. Rev. B **37**, 5571 (1988).

[7]J. L. Pelissier, Phys. Scr. **34**, 838 (1986).

[8]W. Kohn and L. J. Sham, Phys. Rev. **140**, A1133 (1965).

[9]R. Pynn and G. L. Squires, Proc. R. Soc. London Ser. A **326**, 347 (1972).

[10]J. A. Moriarty, Phys. Rev. B **16**, 2537 (1977); **26**, 1754 (1982); **38**, 3199 (1988).

[11]J. D. Althoff, R. M. Wentzcovitch, P. B. Allen, and J. A. Moriarty (unpublished).

[12]S. Ishimaru and K. Utsumi, Phys. Rev. B **24**, 7385 (1981).

[13]W. B. Pearson, *A Handbook of Lattice Spacings and Structures of Metals and Alloys* (Pergamon, New York, 1967).

[14]C. Kittel, *Introduction to Solid State Physics,* 6th ed. (Wiley, New York, 1986).

[15]H. Olijnyk, Phys. Rev. Lett. **68**, 2232 (1992).

[16]H. Olijnyk (private communication); (unpublished).

[17]J. Friedel, J. Phys. (Paris) Lett. **35**, L59 (1974).

[18]D. A. Young and M. Ross, J. Chem. Phys. **74**, 6950 (1981).

[19]R. Rao, Phys. Rev. B **10**, 4173 (1974).

[20]G. K. White, Phys. Lett. **8**, 294 (1964).

[21]W. Hume-Rothery and G. V. Raynor, J. Inst. Metals **65**, 379 (1939).

[22]P. L. Smith, Philos. Mag. **46**, 744 (1955).

[23]K. Raznjevic, *Handbook of Thermodynamic Tables and Charts* (Hemisphere, Washington, 1976).